Nucleation Phase and Dynamic Inversion of the Mw 6.9 Valparaíso 2017 Earthquake in Central Chile

S. Ruiz, Florent Aden-Antoniow, J. C. Baez, C. Otarola, B. Potin, F. del Campo, P. Poli, C. Flores, Claudio Satriano, F. Leyton, et al.

HAL Id: insu-03748835
https://insu.hal.science/insu-03748835

Submitted on 10 Aug 2022

Nucleation Phase and Dynamic Inversion of the M_w 6.9 Valparaíso 2017 Earthquake in Central Chile

S. Ruiz[1], F. Aden-Antoniow[2], J. C. Baez[3], C. Otarola[1,4], B. Potin[3], F. del Campo[3], P. Poli[5], C. Flores[1,4], C. Satriano[2], F. Leyton[3], R. Madariaga[6], and P. Bernard[2]

[1]Geophysics Department, Universidad de Chile, Santiago, Chile, [2]Institut de Physique du Globe de Paris, Paris, France, [3]Centro Sismológico Nacional, Universidad de Chile, Santiago, Chile, [4]Geology Department, Universidad de Chile, Santiago, Chile, [5]Massachusetts Institute of Technology, Cambridge, MA, USA, [6]Ecole Normale Superieure, Paris, France

Abstract The Valparaiso 2017 sequence occurred in the Central Chile megathrust, an active zone where the last mega-earthquake occurred in 1730. Intense seismicity started 2 days before the M_w 6.9 mainshock, a slow trenchward movement was observed in the coastal GPS antennas and was accompanied by foreshocks and repeater-type seismicity. To characterize the rupture process of the mainshock, we perform a dynamic inversion using the strong-motion records and an elliptical patch approach. We suggest that a slow slip event preceded and triggered the M_w 6.9 earthquake, which ruptured an elliptical asperity (semiaxis of 10 km and 5 km, with a subshear rupture, stress drop of 11.71 MPa, yield stress of 17.21 MPa, slip weakening of 0.65 m, and kappa value of 1.98). This earthquake could be the beginning of a long-term nucleation phase to a major rupture, within the highly coupled Central Chile zone where a megathrust earthquake like 1730 is expected.

1. Introduction

An intense precursory activity started 2 days before the M_w 6.9 earthquake occurred in front of Valparaíso in Central Chile, at 21:38:28 (UTC) on 24 April 2017. This area is an active subduction zone where tsunamigenic megathrust earthquakes have occurred in the past (Dura et al., 2015). The largest recognized earthquake during the last five centuries was the magnitude M_w ~9.0, 1730 earthquake, with a rupture length larger than 600 km (Carvajal, Cisternas, & Catalan, 2017; Udías et al., 2012). Other earthquakes of magnitude M_w ~8.0 struck the zone during the last 100 years (Figure 1). In the same zone of the 2017 earthquakes, a magnitude M_w 8.0 occurred on 3 March 1985 (Comte et al., 1986; Ruiz et al., 2011, and references therein). This earthquake was preceded by an intense swarm-type foreshock activity, which started on 21 February 1985 (Comte et al., 1986). Despite a growing body of field observations of precursors (Bouchon et al., 2013; Ellsworth & Beroza, 1995; Kato et al., 2016; Ruiz et al., 2014), the physics of the earthquake nucleation is still poorly understood. Low magnitude foreshocks or slow slip event precursory phenomena have been recently identified in subduction zones, thanks to the densification of seismological instrumentation. For example, in Chile, the GPS and broadband stations have been widely deployed along the coast. This recent increase in instrumentation enabled a detailed study of the Iquique 2014 earthquake M_w 8.2, along with the characterization of a precursory slow slip event accompanied by an intense foreshock activity, thus shedding light on the physics that control earthquake nucleation (Kato et al., 2016; Ruiz et al., 2014; Socquet et al., 2017). Here we took advantage of the excellent multiparametric data recorded in the Valparaiso region to study in detail the nucleation and the rupture dynamic of the M_w 6.9, 2017 earthquake. First, we analyzed the seismicity preceding the mainshock and GPS time series displacement to assess if the M_w 6.9 earthquake was triggered by slow slip on the subduction interface or by a cascade process. We start building a complete seismic catalogue of foreshocks and aftershocks using the continuous time data, we localized manually the largest events, and we computed their moment tensors to accurately define the fault plane of the Valparaiso seismicity sequence. We searched for repeating seismicity in the foreshocks sequence to relate it with possible aseismic movement. Then, we performed a geodetic inversion using the GPS time series displacement measured before the mainshock. Based on this analysis, we were able to quantify the relative amount of aseismic and seismic displacement at the seismogenic contact. Finally, we performed a detailed study of the rupture parameters of the mainshock using a full dynamic inversion. These dynamic parameters have been well studied for intermediate depth earthquakes on subduction zones (Herrera et al., 2017; Ruiz & Madariaga, 2011, 2013); here we provide a first picture of the dynamics of an interplate thrust earthquake in Chile.
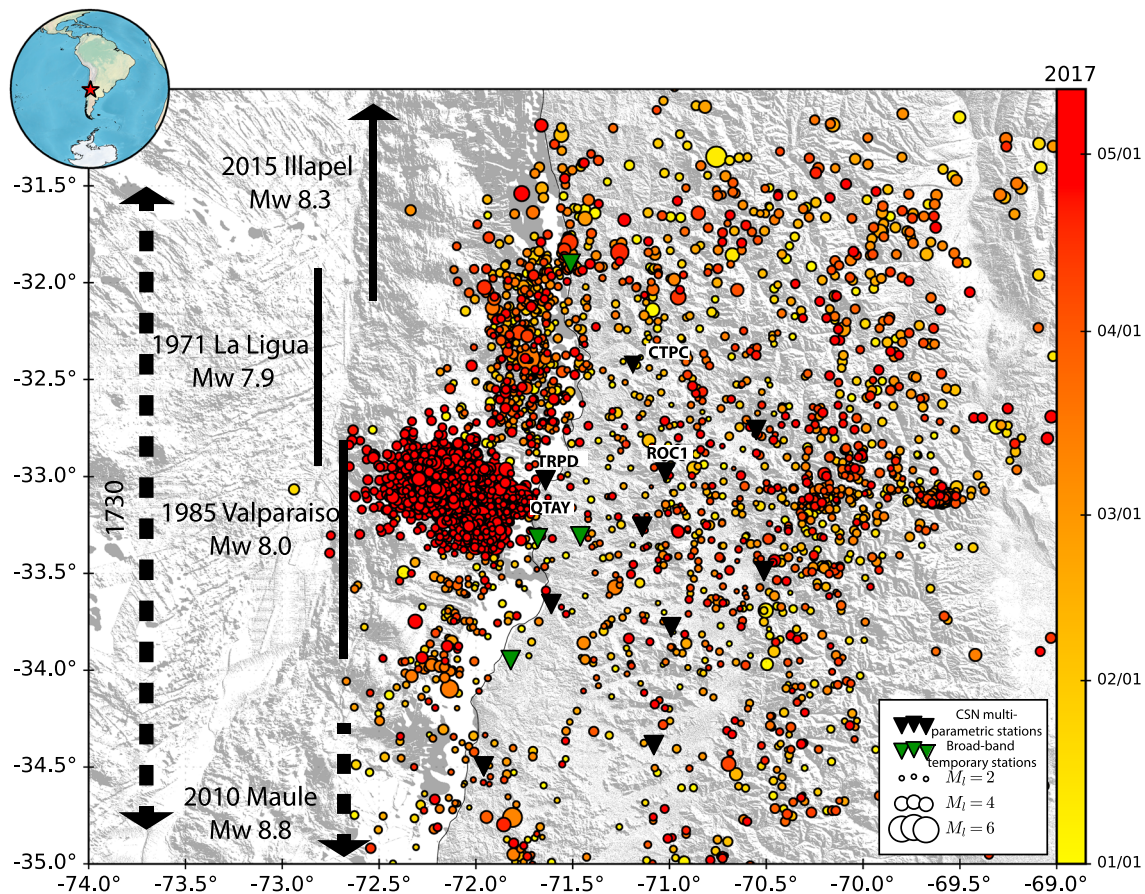
Figure 1. Detected seismicity from 1 January 2017 to 12 May 2017. The largest concentration of earthquakes between latitude −33.0° and −72.2° corresponds to the Valparaíso 2017 sequence. The inverted triangles mark the seismological instruments used in this work: Black corresponds to permanent multiparametric stations, and green corresponds to temporary broadband stations deployed by our group and CSN (National Seismological Center of the University of Chile). Vertical bars show approximately the rupture length of the last interplate earthquakes that occurred in the zone, and the dashed lines are associated with the 2010 and 1730 megathrust ruptures. The code names indicate GPS antennas closest to the Valparaiso earthquakes. Topography from Ryan et al. (2009).

2. Data, Methodology, and Results

The Valparaiso sequence was recorded by the CSN (www.sismologia.cl) on seismological and GPS stations. The first earthquake occurred on 22 April 2017 at 22:46:44 with magnitude M_w 4.8 and was followed by an unusually intense seismicity, including a moderate magnitude earthquake that took place on 23 April 2017 at 02:36:06 (M_w 5.9). The mainshock took place on 24 April, with magnitude M_w 6.9. The aftershocks slightly migrated to the south, with the largest magnitude aftershock occurring on 28 April at 16:05:57 M_w 6.0 (Figures 1 and 2). We first characterize the Valparaiso 2017 seismicity using the broadband seismic records; then we analyze GPS data and show a possible slow slip event occurring before the main shock. Finally, we studied the seismic source rupture of the mainshock using strong motion data.

2.1. Valparaiso Seismicity

In the first step, we developed a 3-D velocity model (3DVM) for Central Chile, roughly between 30°S to 36°S and 68°W to 74°W. The inversion of the arrival times of body waves was carried out using a nonlinear least-squares approach based on the large number law and a stochastic description of both data and model, following Potin (2016). The 3DVM is derived from the arrival times of 114,018 *P* and 96,157 *S* waves corresponding to 11,829 earthquakes in the CSN catalogue that occurred since 2012 (www.sismologia.cl). Then, to better resolve any spatiotemporal evolution of the seismicity, we built a new seismic catalogue from 1 January to 12 May 2017, using the methodology of Poiata et al. (2016). This approach is based on a fourth-
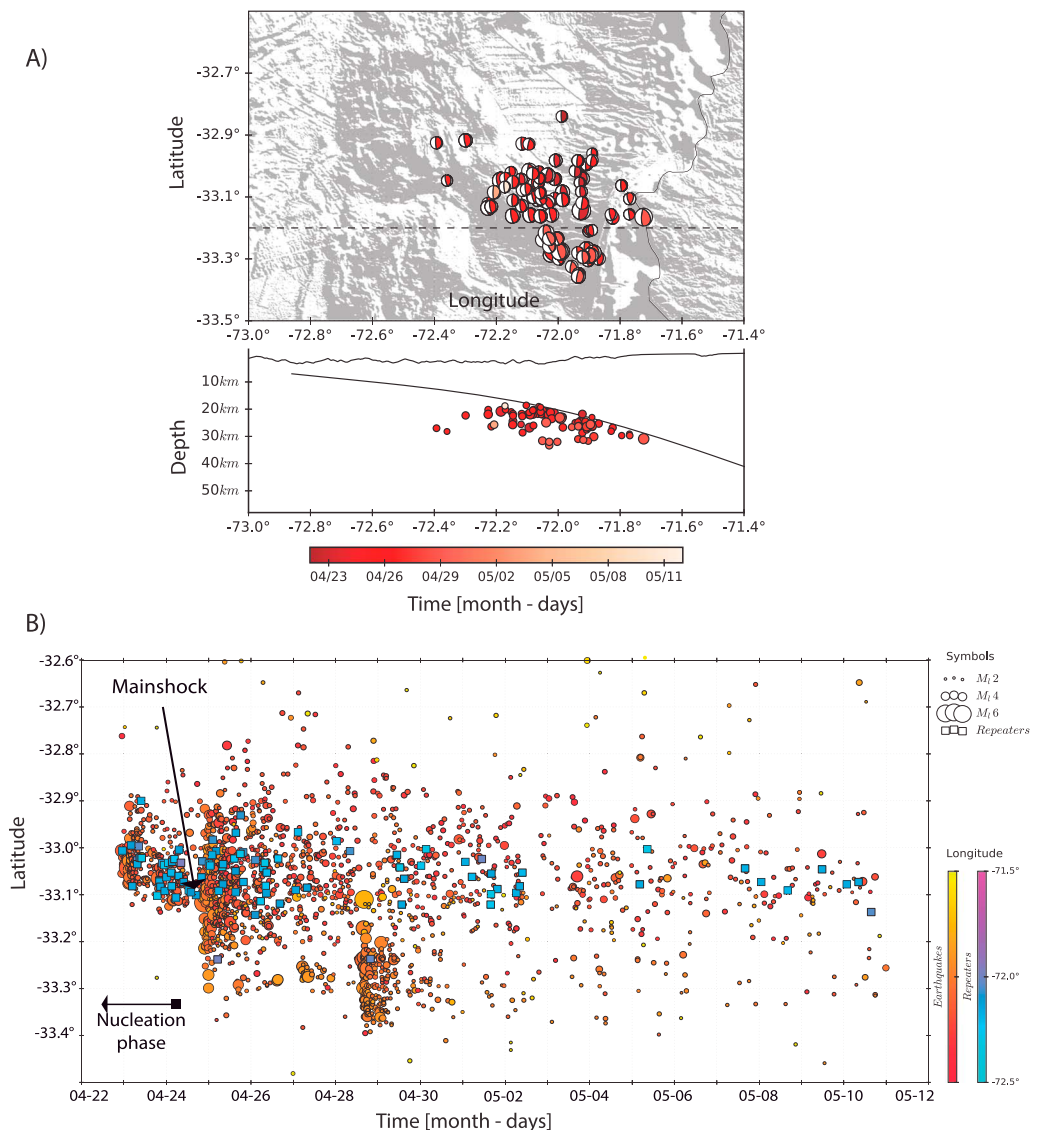
Figure 2. Focal mechanism of earthquakes larger than magnitude 3.5 and seismicity of Valparaiso 2017. (a) The seismicity started at 31.10°S, and after the mainshock, it migrated southward to 32.30°S. All the focal mechanisms correspond to reverse faults. (b) Profile along of the segmented line shown in Figure 2a; dots denote the centroid position. In Figures 2a and 2b, the color bar follows the seismicity–time evolution; the scale is in the middle. (c) Time–latitude evolution of the seismicity detected in this work, from 22 April to 12 May; the seismicity from 1 January is shown in Figure S6. The dots are regular earthquakes, while the squares are repeating earthquakes.

order statistic characterization of the signal in different frequency bands, followed by back-projection and stacking of time-delay functions. Here we used 10 frequency bands between 5 and 50 Hz and a detection threshold of 0.7 for the maximum of the normalized stacked time-delay function.

As a further step, we used the measured phase arrival time from the above analysis to perform a joint relocation using the NonLinLoc program of Lomax et al. (2000). We discarded earthquakes with one axis of the 68%-of-confidence ellipsoid larger than 30 km. The resulting catalogue is composed of 4,356 earthquakes, with 2,329 belonging to the Valparaiso sequence. The completeness magnitude (M_c) is M_L 2.8, significantly lower than that of the CSN catalogue ($M_c = M_L$ 3.8) for the same time period and zone (Figure S1 in the supporting information). After automatic detection and location, we picked P and S waves manually for each earthquake with a local magnitude greater than 3.5 and relocated them with the NonLinLoc code.

We inverted the full moment tensor for each identified earthquakes using the ISOLA code (Sokos & Zaharadnik, 2008; Vackář et al., 2017). We explored for the centroid and the best fitting nondouble couple using a 1 km width (50 m step) grid search around the hypocenter. The selected nondouble couples are kept if they minimized the variance between observed and simulated traces and after a visual check of the waveform compatibility. The data were filtered using a band-pass filter for which we chose, after several tests, corner frequencies of 0.15 and 0.2 Hz, which are considered to be the best to model earthquakes larger than 3.5. A representative 1-D velocity model extracted from our 3DVM velocity model (Table S1) was used to compute synthetics. The location and the computed focal mechanisms of 88 earthquakes suggest an interface-only activity during the sequence (Figures 2a and 2b).

We study the presence of repeating earthquakes using our seismic catalogue, to assess if any aseismic slip acceleration can be observed before the mainshock (e.g., Kato et al., 2016). The repeaters were identified by coherence of vertical component seismograms in a frequency band from 5 to 15 Hz. We used signals from 2 s before up to 10 s after the P waves; given the source to station distance, this window contains P, P coda, and S waves. A repeater is defined when the correlation coefficient at two or more stations exceeds 0.95 (Figure S2). We found 93 repeating earthquakes (Figure 2b), 34 of which occurred before the mainshock in a compact elliptical patch. Following the scaling relationships between slip and magnitude of Nadeau and Johnson (1998), we estimated the slip preceding the main shock using the approach of Kato et al. (2016). The estimated maximum slip before the mainshock is ~6 cm; even more, the analysis of repeaters suggests that an aseismic movement took place before the mainshock. Hence, we decide to use GPS data to further constraint if any aseismic slip is present before the main event.

2.2. Slow and Fast Movements Recorded by the GPS Instruments

The Valparaiso sequence was captured by GNSS stations recording at 1 Hz (Figure 1). These data were processed using Bernese GNSS Software V5.2, including Earth rotation and precise orbit parameters from IGS final products (Dach et al., 2015; Dow et al., 2009). The processing strategy was carried out in two steps: first, we used daily files for each station surrounding the earthquake area, at 15 s rate; 15 selected IGS regional stations were included to estimate the position in daily bases. We used the minimum constraint approach, for the datum definition, and we applied No Net Rotation and No Net Translation conditions for the regional IGS stations. For the second step, we added a selected set of IGS reference stations from the far field and divided all files into 6 h time windows at 1 Hz; we selected this time window through a trial-and-error approach, balancing time resolution and error estimations. The nearest GPS antennas to the Valparaiso earthquakes are stations BN05, TRPD, and VALN located in Valparaiso city and stations QTAY, CTPC, and ROB1 (Figure 1). These time series show an accelerated trenchward movement starting 4 days before the mainshock, Figures 3a, 3b, and S3, which is in agreement with the enhanced amount of repeating earthquakes suggesting a slow deformation. We thus perform static inversion using this data set to better constraint the characteristic of the aseismic slip. From the Valparaiso stations, we only consider station TRPD located on rock; we excluded stations BN05 and VALN because these antennas are located on the roof of three floor buildings. We modeled the slip distribution associated to the displacement that occurred 4 days before the mainshock. During this period, we observed a movement of 1.35 cm to the West in the Valparaiso stations (Figures 3a and 3b) and also an important movement at ROB1 and CTPC. Considering the localization of the foreshocks and their corresponding focal mechanism, we assumed that the slip took place at the seismogenic contact and inverted the observed GPS displacement using a grid discretization following the slab proposed by Tassara and Echaurren (2012; Figure 3c). We computed a seismic moment of 8.4×10^{18} N m (M_w 6.55), considering a shear modulus of 40 GPa and a maximum slip of 9 cm (see Figure 3c). This last value agrees with the 6 cm slip estimated from the repeater analysis. The largest foreshock had a moment magnitude of M_w 6.0 (considering the USGS W phase moment tensor instead of the M_w 5.9 reported by the CSN), and the sum of the seismic moment of foreshocks is close to 1.73×10^{18} N m. Therefore, nearly 80% of seismic moment was aseismic during the nucleation phase.

2.3. Mainshock Seismic Rupture

To characterize the mainshock rupture, we first performed a geodetic inversion of the observed coseismic displacement. The slip distribution solution shows a good fit of the GPS data and a compact slip distribution (Figure S4). Given this a priori information about the final slip distribution of the mainshock, we performed a
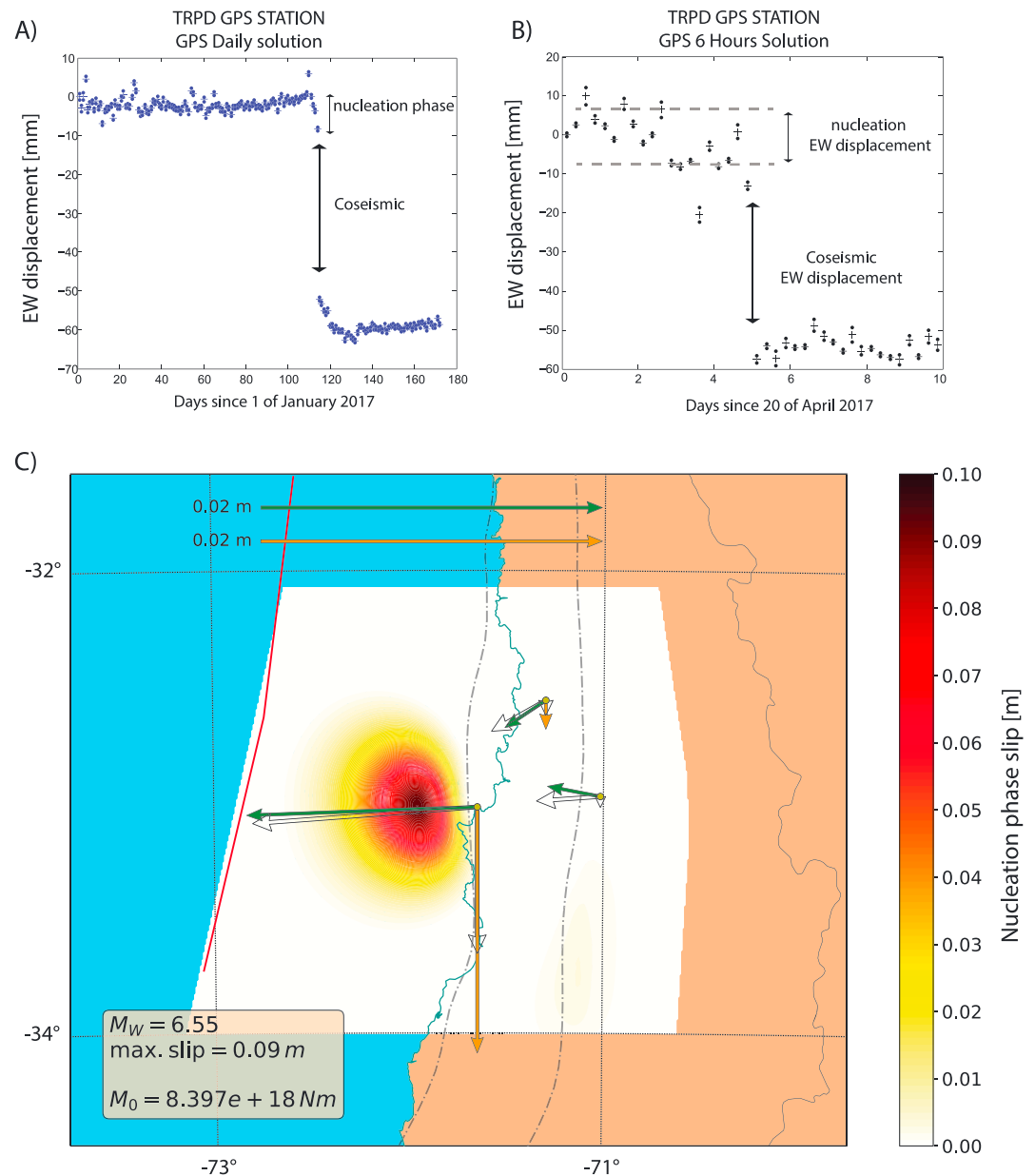
Figure 3. Valparaiso GPS time series and slip distribution of nucleation phase. (a) East–west daily GPS solution for TRPD station. An accelerated movement to west is observed 4 days before mainshock. (b) Six hours GPS solution at TRPD station; the nucleation phase is observed in more detail before the mainshock. (c) Slip distribution inverted considering the 2 day movement detected by the GPS stations; in Figure S3 we show the time series of TRPD, CTPC, and ROB1 GPS stations. The colored arrows are the real GPS vector data, and the transparent arrows are the simulated GPS vectors.

full dynamic inversion considering the ellipse approximation (Ruiz & Madariaga, 2011, 2013), using the strong-motion records from this earthquake (evtdb.csn.uchile.cl). We filtered them between 0.02 Hz to 0.1 Hz, and we integrated twice the traces to compute the dynamic inversion (Figure S6). We inverted for 10 parameters that completely describe the geometry and rupture process of the asperity (see details in Herrera et al., 2017). The frictional parameters are defined by three parameters proposed by Ida (1972): slip weakening distance (D_c), stress drop (T_e), and yield stress (T_u). Wave propagation from source to receivers was computed with the AXITRA code of Bouchon (1981) and Coutant (1989). The velocity model used to generate synthetics is in Table S1. For the inversion, we used an L2 misfit function between
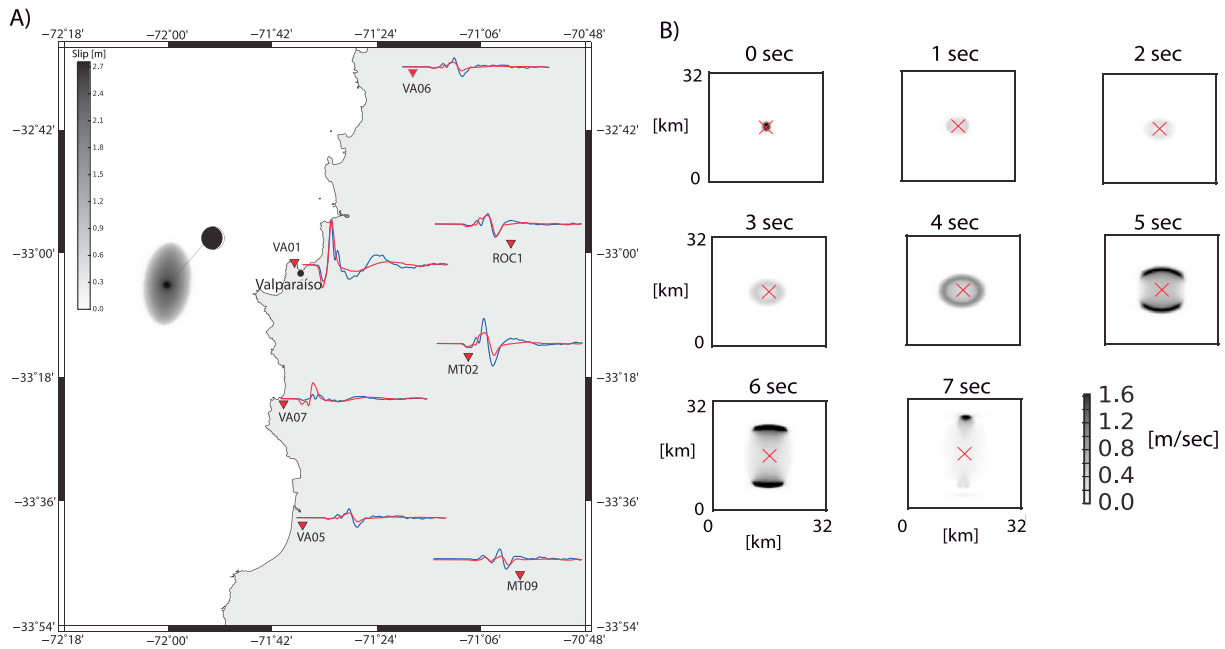
Figure 4. Best model of dynamic inversion of Valparaiso mainshock. (a) Slip distribution obtained from dynamic inversion. Maximum displacement is 2.7 m. The EW components of real (blue) and simulated (red) strong motion records, integrated to displacement, used in the inversion are shown. The NS and UD records are shown in Figure S5. Focal mechanism from W phase moment tensor reported by USGS was used in the inversion. (b) Snapshots taken every second of the slip rate in the fault plane; the seismic rupture has a subshear velocity and a total duration shorter than 8 s.

simulated and observed records. Finally, we computed the similarity parameter κ, defined by Madariaga and Olsen (2000):

$$k = \frac{(T_e - T_r)^2 L}{\mu (T_u - T_r) D_c} \tag{1}$$

where T_e, T_u, and D_c are the parameters of the slip weakening friction law defined by Ida (1972), L is the average size of the rupture area, and μ is the shear modulus. The residual stress T_r is considered to be equal to zero in our definition. k is a nondimensional parameter that controls the dynamic characteristics of the rupture (see details in Madariaga & Ruiz, 2016). The best solution has a misfit of 0.397 with the following dynamic parameter values: stress drop T_e = 11.71 [MPa], yield stress T_u = 17.21 [MPa], D_c = 0.65 [m], and k = 1.98 (Figure 4). These values agree with that observed in other intraplate intermediate depth earthquakes using the same methodology (Herrera et al., 2017, and references therein). The stress drop value obtained here is slightly lower than the intraplate earthquakes, but overall, the slip weakening friction law parameters are well represented by the k parameter, which is of the same order as that obtained for intermediate depth earthquakes.

3. Discussion

The 3 March 1985 Valparaiso foreshocks occurred almost at the same place as that of the sequence studied here, within a zone of 20 km × 40 km; this sequence started on 21 February 1985 when an m_b 4.7 earthquake occurred (Comte et al., 1986). Note that the mainshock M_w 8.0 of Valparaiso earthquake started inside the foreshocks region. There are clear similarities in the seismic process of both 1985 and 2017 earthquakes; the main differences being the magnitude of the main shocks. The simplest explanation for these differences is the cumulative strain occurred in only 32 years for the 2017 earthquake, in comparison with the longer period of quiescence of large magnitude events before 1985. In fact, the previous large earthquake occurred in 1906, a magnitude 8.2 that broke the deeper zone of contact in the Valparaiso region (Carvajal, Cisternas, Gubler, et al., 2017; Okal, 2005). However, the coupling maps for Central Chile zone (Métois et al., 2016; Moreno et al., 2010) show a high value of coupling; which could indicate that the Central Chile zone is prepared for another mega-earthquake. The 2017 sequence could correspond to the beginning of a
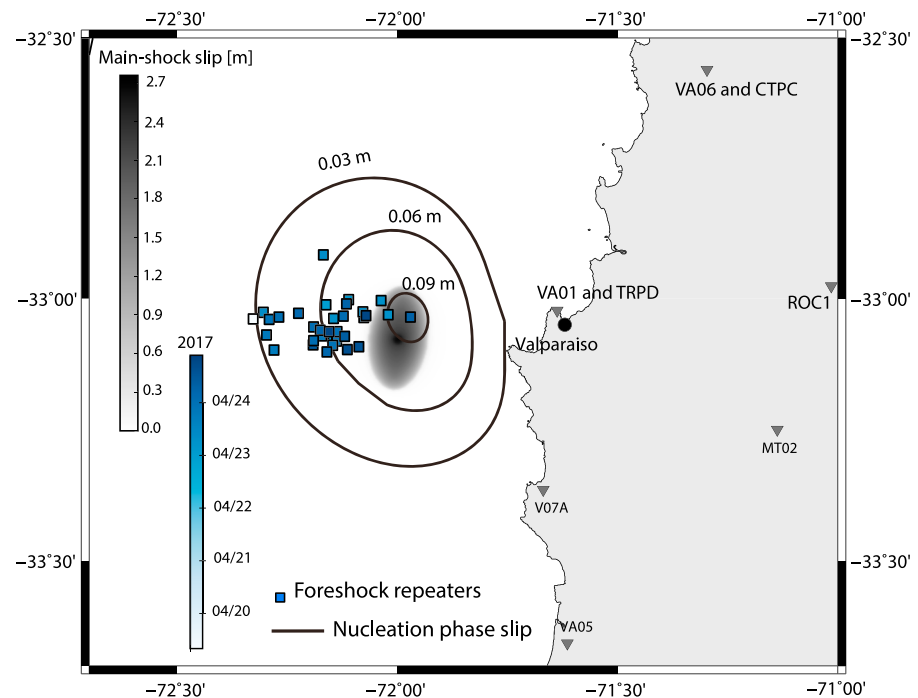
Figure 5. Nucleation phase and mainshock slip distributions, and foreshock repeaters. Continuous lines correspond to the slip distribution obtained from GPS data inversion of the nucleation phase (Figure 3b). The gray dashed zone is the mainshock slip distribution obtained from dynamic inversion of strong motion records (Figure 4a). The foreshock repeaters are color-coded from their time of occurrence.

long-term nucleation phase of a megathrust earthquake. A more conservative hypothesis is that the M_w 6.9 is an isolated earthquake and corresponds to normal seismicity for an area where earthquakes of magnitude about 9 occur every ~400 years.

Two main models of earthquake nucleation have been proposed (e.g., Ellsworth & Beroza, 1995): a cascade process or an aseismic slip where the rupture starts slowly with foreshocks triggered by the slow slip and that accelerates in the final stage triggering the mainshock. In the case of Valparaiso 2017, the slip distribution of the nucleation phase (Figure 3) is concentrated in the same zone where the M_w 6.9 asperity was broken on 24 April 2017 (Figure 5). The repeating earthquakes are located to the west of the mainshock rupture zone. The presence of repeaters and the slip distribution of the nucleation phase, which has an important fraction of aseismic slip, suggest that the mainshock was probably triggered by a slow slip event rather than being the result of a cascade rupture process.

We obtain dynamic parameters for the M_w 6.9 earthquake. The stress drop value obtained here is slightly lower than the intraplate earthquakes; however, the *kappa* value, regrouping the friction law parameters, is of the same order as that obtained for intermediate depth earthquakes, suggesting a similar dynamic rupture process, despite of the different tectonic context.

4. Conclusions

The Valparaiso 2017 seismicity occurred at the interplate contact, where the 1985 and 1906 Valparaiso earthquakes previously occurred, as well as the 1730 mega-earthquake, among others. Two days before the M_w 6.9 main shock, intense seismic activity occurred in the zone. This seismicity was accompanied by an aseismic movement observed with GPS stations and repeater-type seismicity. The nucleation movement took place in the same zone where the main asperity was broken. The M_w 6.9 rupture was characterized by a subshear speed within a slip zone modeled by an elliptical patch of 10 km × 20 km. The aftershock seismicity migrated to southeast surrounding the mainshock. All the above observations lead us to propose that the Valparaiso 2017 earthquake was triggered by a slow slip event.

References

Bouchon, M. (1981). A simple method to calculate Green's functions for elastic layered media. *Bulletin of the Seismological Society of America*, *71*(4), 959–971.

Bouchon, M., Durand, V., Marsan, D., Karabulut, H., & Schmittbuhl, J. (2013). The long precursory phase of most large interplate earthquakes. *Nature Geoscience*, *6*(4), 299–302. https://doi.org/10.1038/ngeo1770

Carvajal, M., Cisternas, M., & Catalan, P. (2017). Source of the 1730 Chilean earthquake from historical records: Implications for the future tsunami hazard on the coast of Metropolitan Chile. *Journal of Geophysical Research: Solid Earth*, *122*, 3648–3660. https://doi.org/10.1002/2017JB014063

Carvajal, M., Cisternas, M., Gubler, A., Catalan, P. A., Winckler, P., & Wesson, R. L. (2017). Reexamination of the magnitudes for the 1906 and 1922 Chilean earthquakes using Japanese tsunami amplitudes: Implications for source depth constraints. *Journal of Geophysical Research: Solid Earth*, *122*, 4–17. https://doi.org/10.1002/2016JB013269

Comte, D., Eisenberg, A., Lorca, E., Pardo, M., Ponce, L., Saragoni, R., … Suarez, G. (1986). The great 1985 Central Chile earthquake: A repeat of previous great earthquakes in the region? *Science*, *299*, 449–453.

Coutant, O. (1989). Programme de simulation numerique AXITRA, Res. Report LGIT, Grenoble, France.

Dach, R., Lutz, S., Walser, P., & Fridez, P. (Eds.) (2015). *Bernese GNSS software version 5.2. User manual*. Astronomical Institute, University of Bern, Bern Open Publishing. https://doi.org/10.7892/boris.72297

Dow, J. M., Neilan, R. E., & Rizos, C. (2009). The International GNSS Service in a changing landscape of Global Navigation Satellite Systems. *Journal of Geodesy*, *83*(3-4), 191–198. https://doi.org/10.1007/s00190-008-0300-3

Dura, T., Cisternas, M., Horton, B., Ely, L., Nelson, A., Wesson, R., & Pilarczyk, J. (2015). Coastal evidence for Holocene subduction-zone earthquakes and tsunamis in Central Chile. *Quaternary Science Reviews*, *113*, 93–111.

Ellsworth, W. L., & Beroza, G. C. (1995). Seismic evidence for a seismic nucleation phase. *Science*, *268*(5212), 851–855. https://doi.org/10.1126/science.268.5212.851

Herrera, C., Ruiz, S., Madariaga, R., & Poli, P. (2017). Inversion of the dynamic parameters of the 2015 Jujuy intermediate depth earthquake, and their values compared with other intraslab earthquakes. *Geophysical Journal International*, *209*(2), 866–875. https://doi.org/10.1093/gji/ggx056

Ida, Y. (1972). Cohesive force across the tip of a longitudinal-shear crack and Griffith's specific surface energy. *Journal of Geophysical Research*, *77*, 3796–3805. https://doi.org/10.1029/JB077i020p03796

Kato, A., Fukuda, J. I., Kumazawa, T., & Nakagawa, S. (2016). Accelerated nucleation of the 2014 Iquique, Chile M_w 8.2 earthquake. *Scientific Reports*, *6*.

Lomax, A., Virieux, J., Volant, P., & Berge, C. (2000). Probabilistic earthquake location in 3D and layered models: Introduction of a Metropolis–Gibbs method and comparison with linear locations. In C. H. Thurber & N. Rabinowitz (Eds.), *Advances in seismic event location*, (pp. 101–134). Amsterdam: Kluwer. https://doi.org/10.1007/978-94-015-9536-0_5

Madariaga, R., & Olsen, K. B. (2000). Criticality of rupture dynamics in 3-D. *Pageoph*, *157*(11), 1981–2001. https://doi.org/10.1007/PL00001071

Madariaga, R., & Ruiz, S. (2016). Earthquake dynamics on circular faults: A review 1970–2015. *Journal of Seismology*, *20*(4), 1235–1252. https://doi.org/10.1007/s10950-016-9590-8

Métois, M., Vigny, C., & Socquet, A. (2016). Interseismic coupling, megathrust earthquakes and seismic swarms along the Chilean subduction zone. *Pure and Applied Geophysics*, *117*(B3), 1431–1449. https://doi.org/10.1007/s00024-016-1280-5

Moreno, M., Rosenau, M., & Oncken, O. (2010). 2010 Maule earthquake slip correlates with pre-seismic locking of Andean subduction zone. *Nature*, *467*(7312), 198–202. https://doi.org/10.1038/nature09349

Nadeau, R. M., & Johnson, L. R. (1998). Seismological studies at Parkfield VI: Moment release rates and estimates of source parameters for small repeating earthquakes. *Bulletin of the Seismological Society of America*, *88*, 790–814.

Okal, E. A. (2005). A re-evaluation of the great Aleutian and Chilean earthquakes of 1906 August 17. *Geophysical Journal International*, *161*(2), 268–282. https://doi.org/10.1111/j.1365-%20246X.2005.02582.x

Poiata, N., Satriano, C., Vilotte, J.-P., Bernard, P., & Obara, K. (2016). Multi-band array detection and location of seismic sources recorded by dense seismic networks. *Geophysical Journal International*, *205*(3), 1548–1573. https://doi.org/10.1093/gji/ggw071

Potin, B. (2016). Les Alpes Occidentales: Tomographie, localisation de séismes et topographie du Moho, PhD thesis, University Grenoble-Alpes (France), ISTerre.

Ruiz, S., Kausel, E., Campos, J., Saragoni, G. R., & Madariaga, R. (2011). Identification of high frequency pulses from earthquake asperities along Chilean subduction zone using strong motion. *Pure and Applied Geophysics*, *168*(1-2), 125–139. https://doi.org/10.1007/s00024-010-0117-x

Ruiz, S., & Madariaga, R. (2011). Determination of the friction law parameters of the M_w 6.7 Michilla earthquake in northern Chile by dynamic inversion. *Geophysical Research Letters*, *38*, L09317. https://doi.org/10.1029/2011GL047147

Ruiz, S., & Madariaga, R. (2013). Kinematic and dynamic inversion of the 2008 northern Iwate earthquake. *Bulletin of the Seismological Society of America*, *103*(2A), 694–708. https://doi.org/10.1785/010120056

Ruiz, S., Metois, M., Fuenzalida, A., Ruiz, J., Leyton, F., Grandin, R., … Campos, J. (2014). Intense foreshocks and a slow slip event preceded the 2014 Iquique M_w 8.1 earthquake. *Science*, *345*(6201), 1165–1169. https://doi.org/10.1126/science.1256074

Ryan, W. B. F., Carbotte, S. M., Coplan, J. O., O'Hara, S., Melkonian, A., Arko, R., … Zemsky, R. (2009). Global multi-resolution topography synthesis. *Geochemistry, Geophysics, Geosystems*, *10*, Q03014. https://doi.org/10.1029/2008GC00233

Socquet, J. P. V., Jara, J., Cotton, F., Walpersdorf, A., Cotte, N., Specht, S., … Norabuena, E. (2017). An 8-month slow slip event triggers progressive nucleation of the 2014 Chile megathrust. *Geophysical Research Letters*, *44*, 4046–4053. https://doi.org/10.1002/2017GL073023

Sokos, E. N., & Zahradnik, J. (2008). ISOLA—A Fortran code and a Matlab GUI to perform multiple-point source inversion of seismic data. *Computational Geosciences*, *34*(8), 967–977. https://doi.org/10.1016/j.cageo.2007.07.005

Tassara, A., & Echaurren, A. (2012). Anatomy of the Andean subduction zone: Three-dimensional density model upgraded and compared against global-scale models. *Geophysical Journal International*, *189*, 161–168.

Udías, A., Madariaga, R., Buforn, E., Muñoz, D., & Ros, M. (2012). The large Chilean historical earthquakes of 1647, 1657, 1730, and 1751 from contemporary documents. *Bulletin of the Seismological Society of America*, *102*(4), 1639–1653. https://doi.org/10.1785/0120110289

Vackář, J., Gallovič, F., Burjánek, J., Zahradník, J., & Clinton, J. (2017). Bayesian ISOLA: New tool for automated centroid moment tensor inversion. *Geophysical Journal International*, *210*(2), 693–705. https://doi.org/10.1093/gji/ggx158